RESEARCH MEMORANDUM

THRUST AND PUMPING CHARACTERISTICS OF A SERIES OF EJECTOR-TYPE EXHAUST NOZZLES AT SUBSONIC AND SUPERSONIC FLIGHT SPEEDS

By Donald P. Hearth and Alfred S. Valerino

Lewis Flight Propulsion Laboratory
Cleveland, Ohio

NATIONAL ADVISORY COMMITTEE
FOR AERONAUTICS

WASHINGTON

November 17, 1954

NACA RM E54H19

NATIONAL ADVISORY COMMITTEE FOR AERONAUTICS

RESEARCH MEMORANDUM

THRUST AND PUMPING CHARACTERISTICS OF A SERIES OF EJECTOR-TYPE EXHAUST NOZZLES AT SUBSONIC AND SUPERSONIC FLIGHT SPEEDS

By Donald P. Hearth and Alfred S. Valerino

SUMMARY

An investigation was conducted in the 8- by 6-foot supersonic wind tunnel to determine the thrust and pumping characteristics of a series of ejector exhaust nozzles. Data were obtained for various ejector diameter and spacing ratios at free-stream Mach numbers of 0.10, 0.63, 1.50, and 1.90 over a pressure-ratio range of 1 to 10 and secondary-primary weight-flow ratios to 0.36.

Results of this investigation indicated that free-stream Mach number had no effect on the pumping and jet-thrust characteristics of the ejectors in the range for which the secondary flow was choked. The mass-flow discharge coefficient of the primary nozzle was reduced as secondary weight flow was increased for some of the shroud configurations. However, the flow coefficient was not affected by primary pressure ratio or free-stream Mach number.

INTRODUCTION

It has been shown (refs. 1 and 2) that increases in the basic thrust of a conventional convergent nozzle may be obtained when cooling air is pumped through an ejector surrounding the primary nozzle. These ejector-type exhaust nozzles also represent a form of variable-geometry jet exit (ref. 2) which is desirable for engine operation over a wide range of pressure ratios. Numerous investigations (refs. 3 and 4, for example) have been made in quiescent air to determine the thrust and pumping characteristics of various types of ejector nozzles.

In order to fully evaluate such exhaust systems, determination of the interferences between the internal and external flows are required. Investigation of this problem has been initiated; results concerning the external flow influence on ejector pumping performance and the external drag characteristics are reported in references 5 and 6. However, the external flow effect on measured internal thrust for ejector configurations has not been reported.

To provide information concerning this problem, an investigation was conducted in the NACA 8- by 6-foot supersonic wind tunnel on a series of ejector-type exhaust nozzles proposed for use on supersonic airplanes. Gross-thrust data, as well as the pumping characteristics, are presented for various ejectors at free-stream Mach numbers of 0.10, 0.63, 1.50, and 1.90 and at primary pressure ratios of 1 to 10. The secondary weight flow was varied from zero to 36 percent of the primary weight flow. The primary nozzle was set for simulated afterburner-on operation. Analyses of these data were made to provide an over-all comparison of the various configurations and also to compare the net-thrust-augmentation characteristics of the ejectors to those of conventional nozzles.

APPARATUS AND PROCEDURE

Installation

The ejector configurations were mounted on an exit model which was installed in the 8- by 6-foot supersonic wind tunnel, as shown in figures 1 and 2. Air preheated to 250° F was introduced into the model by means of the two hollow support struts shown. Although a can-type combustor was installed in the exit model (fig. 3), all data were obtained without a hot primary jet.

Shown schematically in figure 3 are the internal details of the exit model. For the purposes of the present investigation, the external afterbody was gradually tapered from the maximum body diameter of 8.25 inches at station 49.25 to a diameter of 5.86 inches at station 70.61. The external shrouds investigated were mounted at this station. A simulated vertical fin was mounted on the afterbody as indicated. The combustor, bleed valve (for varying the secondary weight flow), and inner liner were attached internally to the outer shell. A more detailed discussion of the basic exit model and its installation in the tunnel is included in reference 7.

Ejector Configurations

Presented in figure 4 are schematic drawings and tables of internal coordinates for the various external shroud configurations. All the configurations were investigated with the same primary nozzle, the throat diameter of which was 3.75 inches. This sonic nozzle represented the afterburner-on case (nozzle-entrance diameter, 4.10 in.), where the collar shown simulated the mechanism for varying the nozzle-throat area.

The various ejectors are designated by two numbers; the first refers to the diameter ratio, while the second refers to the spacing ratio. The "basic configuration" had a diameter ratio d_s/d_p of 1.16

[redacted]

and a spacing ratio S/dp of 0.80. Ejector 1.16-0.80-S consisted of the basic configuration with simulated stiffener rings installed on the inside of the shroud downstream of the primary nozzle such that the exit shroud diameter was not restricted. Cutting 0.98 inch from the mixing length of the basic ejector resulted in an ejector (1.29-0.54) having a larger diameter ratio and a smaller spacing ratio. The base bleed configuration, ejector 1.48-0, was obtained by cutting the basic ejector at the plane of the nozzle exit so that the diameter ratio was 1.48. Ejector 1.16-0.38, which had the same diameter ratio but a smaller spacing ratio than the basic configuration, was obtained by increasing the boattailing of the external shroud.

Data Reduction

Symbols are defined in appendix A. The method of thrust measurement is described in appendix B. This method differs from that of reference 7 in that the momentum of the entering nozzle air was measured by the strain gage along with the external body drag and the internal drag. Thus, the balance measured the jet thrust minus external drag directly.

Gross ejector force F_e is defined as the jet thrust minus total external drag for the given configuration plus the jet-off external drag of the basic configuration. This latter value was obtained from the balance with no flow passing through the basic configuration. Thus, the gross ejector force for any given configuration consisted of its jet thrust, the change in external drag due to the jet exhaust, and any difference in jet-off external drag between that of the configuration under consideration and the basic configuration. Such a parameter permitted an over-all comparison of the configuration. Force data are presented in terms of the primary nozzle-jet thrust (fig. 5), which was obtained from a thrust calibration with the primary nozzle only installed on the exit model. A check of the force data on a bench test indicated accuracy to ±2 percent.

Total weight flow through the nozzle was obtained from the sharp-edged orifice shown in figure 1 and a rotameter which measured the preheater fuel flow. Primary-nozzle weight flow W_p was calculated by subtracting the amount of weight flow through the calibrated bleed valve W_s from the total weight flow. Primary-nozzle total pressure P_p was obtained from continuity relations at the nozzle entrance where the weight flow, the static pressure, the area, and the total temperature (measured in the support struts and assumed constant throughout the model) were known. Secondary total pressure P_s was measured by means of the total-pressure rake shown in figure 3. Mass-flow coefficients for the primary nozzle, defined as the ratio of actual to ideal mass flow, were calculated with the equation shown in appendix A and are accurate to ±1 percent.

DISCUSSION OF RESULTS

Primary-Nozzle Mass-Flow Coefficients

The effects of free-stream Mach number and pressure ratio on the primary-nozzle mass-flow coefficient are indicated in figure 6. Data are presented only for the basic configuration, ejector 1.16-0.80-S, since the same effects were obtained for the other configurations. As noted in reference 5 for a cylindrical ejector and in references 7 and 8 for other types of nozzles, there was little or no effect of either free-stream Mach number or pressure ratio on the primary-nozzle mass-flow coefficient.

Figure 6 does indicate, however, that there was an effect of secondary weight flow on the mass-flow coefficient. This trend, which was also noted in reference 5, can best be seen in figure 7 in which data for all five configurations are presented as a function of only the secondary weight-flow parameter $\frac{W_s\sqrt{T_s}}{W_p\sqrt{T_p}}$. As indicated, all the configurations yielded the same mass-flow coefficient, 0.995, for secondary weight-flow ratios up to 0.15. Above this amount of bleed, however, the secondary flow appeared to have restricted the primary nozzle for ejectors 1.16-0.80, 1.16-0.80-S, and 1.16-0.38, and the flow coefficient decreased rapidly. No decrease was noted for ejector 1.48-0 in the range for which data were obtained $\left(\text{up to } \frac{W_s\sqrt{T_s}}{W_p\sqrt{T_p}} = 0.27\right)$. A small effect on ejector 1.29-0.54 occurred at the very high amounts of bleed. Thus, ejector diameter ratio appears to have been the governing criterion on this phenomenon.

A one-dimensional analysis of this phenomenon has been made in reference 9 in which it was assumed that equal static pressures exist at the primary nozzle and the shroud exits, and that isentropic flow exists in the primary and secondary flows. By applying these assumptions to continuity relations, contraction of the primary-nozzle vena contracta due to excess secondary flow can be determined as a function of the various physical areas. The mass-flow coefficients obtained by this analysis are shown in figure 7 for all configurations. Although very good agreement of absolute values was obtained, it is probably more significant that the analysis adequately predicted the amount of secondary weight flow at which further increases in bleed flow would result in reduction of the primary-nozzle mass-flow coefficient.

Performance Comparison of Configurations

Pumping and gross ejector force data for all the configurations are presented in figure 8 at free-stream Mach numbers of 0.10, 0.63, 1.50, and 1.90. Secondary-primary total-pressure ratio P_s/P_p and gross ejector force ratio $\frac{F_e}{F_{j,p}}$ are shown as a function of the weight-flow parameter $\frac{W_s\sqrt{T_s}}{W_p\sqrt{T_p}}$ for constant values of primary pressure ratio P_p/p_0.

Pumping characteristics. - These data indicate that cutting back the contour of the basic external shroud to obtain ejectors 1.29-0.54 and 1.48-0 from 1.16-0.80 resulted generally in an improvement in the pumping characteristics, that is, for the same total-pressure ratio, more secondary weight flow was obtained. This advantage increased with bleed flow and primary pressure ratio but was lost at the very low values of these operating conditions. Ejector 1.16-0.38, for which the diameter ratio of the basic configuration was maintained at a smaller mixing length, exhibited essentially the same pumping characteristics as the basic ejector. Thus, the improved pumping for the cut-back configurations is believed to have been due to the increase in minimum secondary-flow area.

Gross ejector force characteristics. - A comparison of the various configurations on an over-all (thrust minus drag) basis is made in figure 8 by the use of the gross ejector force ratio $F_e/F_{j,p}$. The gross ejector force has been defined as the thrust minus drag obtained from the balance plus the jet-off external drag of the basic configuration. Thus, this parameter includes the jet thrust of that configuration, any difference between the jet-off external drag of the configuration under consideration and that of the basic ejector, and the change in external drag due to the jet exhaust.

These data (fig. 8) indicate that the gross ejector force characteristics of the basic configuration were improved by cutting the shroud back about one-third of the mixing length, which resulted in a larger diameter ratio. This improvement was more noticeable at the high primary pressure ratios and/or high secondary weight flows. Slight improvement was also obtained by reducing the mixing length of the basic shroud without changing the diameter ratio (achieved by increasing the amount of external boattailing). The simulated stiffener rings had no effect on the basic ejector pumping characteristics and little effect on the force characteristics except in the very low pressure-ratio range.

The trends shown in figure 8 are influenced by the effect of secondary weight flow on the primary nozzle shown in figure 7. Because ejectors 1.29-0.54 and 1.48-0 did not have a decreasing primary-nozzle mass-flow coefficient, it would be expected that the gross ejector force ratio for these configurations would increase relative to the other configurations as secondary weight flow was increased.

Effect of Free-Stream Mach Number on Ejector 1.16-0.80-S

To determine the influence of free-stream Mach number on ejector performance, the data for the various configurations as presented in figure 8 have been cross-plotted as a function of primary pressure ratio. Presented in figure 9, as an example of these cross plots, is the variation of the gross ejector force ratio for the basic configuration, ejector 1.16-0.80-S, at weight-flow ratios of 0.05, 0.10, 0.15, and 0.30. This figure indicates that except for the anomalous 4.4 pressure-ratio data at Mach number 1.50, there appears to have been no effect of free-stream Mach number, although the gross ejector force parameter shown consisted of external drag changes (due to the jet) as well as the nozzle-jet thrust.

In order to show effects on only the jet thrust, it was necessary to subtract the interference drag from the gross ejector force. Sufficient instrumentation was not installed on the model in the present investigation to determine the change in drag due to the jet. However, an investigation of the same external shroud configuration, but with a smaller primary nozzle, has been conducted for which changes in external drag were obtained. Although the drag characteristics for the two investigations may not have been exactly the same, as a first approximation, the drag values obtained with the smaller primary nozzle (fig. 10) were used. The resulting jet thrust ratios are shown in figure 11 and agree within ±2 percent with the results of a quiescent air investigation (ref. 10) of conical shroud ejectors with approximately the same spacing ratio and diameter ratios.

Included in figure 11 are the pumping characteristics for ejector 1.16-0.80-S obtained from cross-plotting figure 8. The secondary-to-primary total-pressure ratio P_s/P_p decreased for increasing primary pressure ratio until the secondary flow "choked" (reached sonic velocity in the secondary passage (see ref. 11)). Above this value of primary pressure ratio (approximately 3.0), the secondary total pressure remained constant.

Figure 11 indicates no effect of free-stream Mach number on either the pumping characteristics or the ejector jet thrust characteristics. Similar results were obtained by cross-plotting the data of the other configurations. The absence of free-stream Mach number effects is

probably due to secondary flow choking over the pressure ratio range investigated at supersonic free-stream conditions (except 1.48-0 for which no supersonic data were obtained). Supersonic external flow could possibly influence internal ejector performance if the secondary flow were unchoked, as was noted in reference 12 for a base bleed configuration.

Net Thrust Characteristics for Ejector 1.16-0.80-S

Although figure 11 indicated a continued increase of ejector jet thrust with secondary weight flow, the net effect of bleed, if free-stream air is utilized in the ejector, can only be shown if the inlet momentum of the secondary flow is considered. Therefore, net thrust ratios $\frac{F_{n,e}}{F_{n,p}}$ (fig. 12) were calculated in which the total inlet momentum of the primary and secondary flow was subtracted from the ejector jet thrust and the primary-flow inlet momentum was subtracted from the primary jet thrust. This parameter was computed from the ejector jet thrust ratio as shown in appendix C. The following assumptions were made:

(1) Altitude = 35,000 feet

(2) $T_s = T_0$

(3) $T_p = 3500^\circ$ R

The general results were not influenced by the values assumed. Also shown in figure 12 are the maximum secondary weight flows obtainable for inlet pressure recoveries P_s/P_0 of 1.00 and 0.50. Since weight flows above those shown for 100 percent recovery could not be obtained without compressor bleed, calculations of the net thrust ratio were terminated at $P_s/P_0 = 1.00$.

For the supersonic Mach numbers, an optimum bleed flow is evident. As would be expected, the value of the optimum bleed decreased as Mach number was increased because of the increasing inlet momentum penalty of the secondary flow. The maximum bleed flow ($P_s/P_0 = 1.0$) increased as free-stream Mach number was increased because of the higher potential ram recovery of the secondary flow. The maximum obtainable pressure recovery, of course, would be less than 1.0 and would decrease as free-stream Mach number was increased, thereby influencing the maximum secondary flows that could be obtained.

Comparison with Conventional Nozzles

Presented in figure 13 is the variation of the net thrust ratio $\frac{F_{n,e}}{F_{n,p}}$ with primary-nozzle pressure ratio for ejectors 1.16-0.80-S and 1.29-0.54. These curves are for a weight-flow ratio of 0.15, or, if the flow were limited by pressure recovery, for that weight flow at $P_s/P_0 = 1.00$.

Figure 13 indicates the attainment of net jet augmentation over the convergent primary nozzle at subsonic free-stream conditions. At supersonic Mach numbers, however, the net thrust augmentation decreased and in some instances a penalty resulted. This trend was a result of the larger penalty encountered in taking secondary flow aboard. The better performance of the 1.29-0.54 configuration compared with the 1.16-0.80-S configuration at the higher pressure ratios is probably due to the increased diameter ratio (ref. 2).

Reexpansion of the convergent primary nozzle would also cause thrust augmentation. The maximum net thrust augmentation obtained in this manner would result from complete isentropic expansion of the primary flow in a variable expansion ratio nozzle. This case is indicated in figure 13 by the dashed curve, where the jet thrust was obtained by adding to the calibrated primary jet thrust the divergent thrust increment for complete isentropic expansion (ref. 13). It would appear that, within the accuracy of the ejector force data shown in figure 13, a fixed ejector would have net thrust augmentation features comparable with those of a variable convergent-divergent nozzle. The comparison shown in figure 13 could, of course, be altered by the matching of an auxiliary inlet to the ejectors as well as the inlet external drag.

The amount of jet thrust developed by the ejector is compared in figure 14 with the maximum or ideal jet thrust which could possibly be realized by the primary and secondary flows independently. The ideal thrust for each of the two systems is defined (same as in ref. 2) as the product of the mass flow and the ideal velocity resulting from complete isentropic expansion at the given pressure ratio (P_p/p_0 or P_s/p_0). This figure indicates a peak value of approximately 0.985 at a pressure ratio of 4.0 with 10 percent bleed flow. The parameter shown in figure 13 may be useful for comparison with conventional nozzles if the cooling air pumped through the ejector was obtained from the engine rather than from free stream. The peak obtained with this ejector was approximately the same as for a convergent-divergent nozzle (ref. 14).

SUMMARY OF RESULTS

The following results were obtained from an investigation conducted on a series of ejector configurations with the primary nozzle in the afterburner-on position at free-stream Mach numbers of 0.10, 0.63, 1.50, and 1.90 over a pressure-ratio range of 1 to 10 and secondary-to-primary weight-flow ratios to 0.36:

1. Free-stream Mach number had no effect on either the measured jet thrust or pumping characteristics in the range for which the secondary flow was choked.

2. Neither free-stream Mach number nor primary pressure ratio had any effect on the mass-flow coefficient of the primary nozzle. For the smaller diameter ratio configurations, however, a decrease in the flow coefficient resulted from an increase in secondary weight flow.

Lewis Flight Propulsion Laboratory
National Advisory Committee for Aeronautics
Cleveland, Ohio, August 20, 1954

APPENDIX A

SYMBOLS

The following symbols are used in this report:

A	area, sq ft
B	strain-gage-balance reading, lb
C_D	boattail drag coefficient, $\frac{D_b}{q_0 A_m}$
$C_{F_{j,p}}$	ratio of measured primary to computed sonic jet thrust
C_f	mass-flow discharge coefficient, $\frac{W_p}{P_p A_p \left(\frac{2}{\gamma+1}\right)^{\frac{\gamma+1}{2(\gamma-1)}} \sqrt{\frac{\gamma g}{RT_p}}}$
D_{jo}	jet-off external drag, lb
D'_{jo}	jet-off external drag for basic configuration, lb
D_i	reduction of external drag due to jet exhaust (interference drag), $D_{jo} - D_{j,e}$
$D_{j,e}$	total external drag, $D_{jo} - D_i$, lb
$\frac{ds}{dp}$	ejector diameter ratio
F_e	gross ejector force, $F_{j,e} + D_i + (D'_{jo} - D_{jo})$, lb
F_j	jet thrust, $mV + A\Delta p$, lb
$F_{j,e}$	ejector jet thrust, lb
$F_{j,p}$	primary jet thrust, lb
$F_{n,e}$	ejector net thrust, $F_{j,e} - (m_s V_s + m_p V_0)$, lb
$F_{n,p}$	primary net thrust, $F_{n,e} - m_p V_0$, lb

g	acceleration due to gravity, 32.2 ft/sec^2
J	total momentum, $mV + Ap$, lb
M	Mach number
m	mass flow, ρAV, slug/sec
P	total pressure, lb/sq ft
$\frac{P_s}{P_p}$	secondary-to-primary total-pressure ratio
p	static pressure, lb/sq ft
$\frac{P_p}{p_0}$	primary-nozzle pressure ratio
q	dynamic pressure, $\gamma pM^2/2$, lb/sq ft
S	mixing length, in.
$\frac{S}{dp}$	spacing ratio
T	total temperature, $^\circ$R
t	static temperature, $^\circ$R
V	velocity, ft/sec
W	weight flow, lb/sec
$\frac{W_s\sqrt{T_s}}{W_p\sqrt{T_p}}$	weight-flow ratio
γ	ratio of specific heats for air
ρ	static density, slug/cu ft

Subscripts:

i	ideal, complete expansion to free-stream static pressure
m	maximum

p	primary
s	secondary
0	free stream

APPENDIX B

EVALUATION OF EJECTOR FORCES FROM BALANCE

The strain-gage balance was connected to the model as shown schematically in the following sketch:

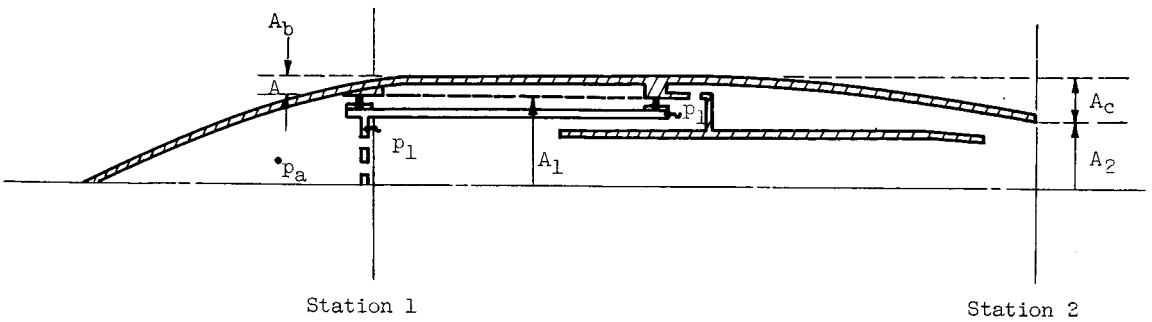

Ejector jet thrust is defined as

$$F_{j,e} = F_2 = mV_2 + p_2A_2 - p_0A_2 \tag{B1}$$

Equation (B1) is equivalent to

$$F_{j,e} = J_2 - p_0A_2 \tag{B2}$$

The momentum at station 2 is related to the momentum at station 1 by

$$J_2 = J_1 - \Delta J_{1-2} \tag{B3}$$

Since

$$J_1 = p_1A_1$$

equation (B2) becomes

$$F_{j,e} = p_1A_1 - \Delta J_{1-2} - p_0A_2 \tag{B4}$$

The strain-gage balance as indicated on the sketch measured the following:

$$B = p_aA_1 + p_0A_c - p_0A_1 - p_0A_b - D_{j,e} - \Delta J_{1-2} \tag{B5}$$

Substitution of ΔJ_{1-2} from equation (B5) into equation (B4) yields

$$F_{j,e} = p_1 A_1 + B + p_0 A_1 + D_{j,e} + p_0 A_b - p_a A_1 - p_0 A_c - p_0 A_2 \quad \text{(B6)}$$

Since $A_1 + A_b = A_c + A_2$

$$F_{j,e} - D_{j,e} = B + A_1(p_1 - p_a) \quad \text{(B7)}$$

Thus, the ejector jet thrust minus the total external drag was measured by the balance and was calculated as shown in equation (B7).

Gross ejector force is defined as

$$F_e = (F_{j,e} - D_{j,e}) + D'_{jo} \quad \text{(B8)}$$

since for any configuration,

$$D_{j,e} = D_{jo} - D_i \quad \text{(B9)}$$

The gross ejector force and ejector jet thrust are, therefore, related as

$$F_e = F_{j,e} + D_i + (D'_{jo} - D_{jo}) \quad \text{(B10)}$$

The gross ejector force and ejector jet thrust have been presented as a function of the calibrated jet thrust of the primary nozzle:

$$\frac{F_e}{F_{j,p}} \quad \text{and} \quad \frac{F_{j,e}}{F_{j,p}}$$

APPENDIX C

EVALUATION OF NET THRUST RATIO

Ejector net thrust and primary net thrust have been defined as:

$$F_{n,e} = F_{j,e} - (m_p V_0 + m_s V_s) \tag{C1}$$

$$F_{n,p} = F_{j,p} - m_p V_0 \tag{C2}$$

The net thrust ratio can thus be written as:

$$\frac{F_{n,e}}{F_{n,p}} = \frac{\frac{F_{j,e}}{F_{j,p}} - \frac{m_p V_0}{F_{j,p}} \left[1 + \left(\frac{V_s}{V_0} \right) \left(\frac{W_s \sqrt{T_s}}{W_p \sqrt{T_p}} \right) \sqrt{\frac{T_p}{T_s}} \right]}{1 - \frac{m_p V_0}{F_{j,p}}} \tag{C3}$$

The momentum term can be written as ($M_p = 1.0$):

$$\frac{m_p V_0}{F_{j,p}} = \frac{p_0 A_p \left[\sqrt{\gamma_p \gamma_0} \left(\frac{P_p}{p_0} \right) (M_0) \sqrt{\frac{t_0}{T_p}} \left(1 + \frac{\gamma_p - 1}{2} \right)^{-\frac{\gamma_p + 1}{2(\gamma_p - 1)}} \right]}{p_0 A_p \left[\gamma_p \left(1 + \frac{\gamma_p - 1}{2} \right)^{-\frac{\gamma_p}{\gamma_p - 1}} \left(\frac{P_p}{p_0} \right) + \left(1 + \frac{\gamma_p - 1}{2} \right)^{-\frac{\gamma_p}{\gamma_p + 1}} \left(\frac{P_p}{p_0} \right) - 1 \right] C_{F_{j,p}}} \tag{C4}$$

where $C_{F_{j,p}}$ is the calibrated thrust coefficient $\left(\frac{\text{measured}}{\text{computed sonic}} \right)$ of the primary nozzle and is included so that the momentum term is based on the same jet thrust as the ejector jet thrust ratio. Thus, the net thrust ratio was calculated for a given M_0, $\frac{W_s \sqrt{T_s}}{W_p \sqrt{T_p}}$, $\frac{P_p}{p_0}$, and $\frac{F_{j,e}}{F_{j,p}}$ by making the following assumptions:

(1) Altitude = 35,000 ft

(2) $T_p = 3500^{\circ}$ R

(3) $T_s = T_0$

(4) $V_s = V_0$

REFERENCES

1. Samuels, John C., and Yanowitz, Herbert: Analysis of Several Methods of Pumping Cooling Air for Turbojet-Engine Afterburners. NACA RM E52K26, 1953.

2. Fleming, William A.: Internal Performance of Several Types of Jet-Exit Configurations for Supersonic Turbojet Aircraft. NACA RM E52K04, 1953.

3. Greathouse, W. K.: Preliminary Investigation of Pumping and Thrust Characteristics of Full-Size Cooling-Air Ejectors at Several Exhaust-Gas Temperatures. NACA RM E54A18, 1954.

4. Huntley, S. C., and Yanowitz, Herbert: Pumping and Thrust Characteristics of Several Divergent Cooling-Air Ejectors and Comparison of Performance with Conical Cylindrical Ejectors. NACA RM E53J13, 1954.

5. Gorton, Gerald C.: Pumping and Drag Characteristics of an Aircraft Ejector at Subsonic and Supersonic Speeds. NACA RM E54D06, 1954.

6. Allen, John L.: Pumping Characteristics for Several Simulated Variable-Geometry Ejectors with Hot and Cold Primary Flow. NACA RM E54G15, 1954.

7. Hearth, Donald P., and Gorton, Gerald C.: Investigation of Thrust and Drag Characteristics of a Plug-Type Exhaust Nozzle. NACA RM E53L16, 1954.

8. Fradenburgh, Evan A., Gorton, Gerald C., and Beke Andrew: Thrust Characteristics of a Series of Convergent-Divergent Exhaust Nozzles at Subsonic and Supersonic Flight Speeds. NACA RM E53L23, 1954.

9. Kochendorfer, Fred D.: Note on Performance of Aircraft Ejector Nozzles at High Secondary Flows. NACA RM E54F17a, 1954.

10. Greathouse, W. K., and Hollister, D. P.: Preliminary Air-Flow and Thrust Calibrations of Several Conical Cooling-Air Ejectors with a Primary to Secondary Temperature Ratio of 1.0. I - Diameter Ratios of 1.21 and 1.10. NACA RM E52E21, 1952.

11. Kochendorfer, Fred D., and Rousso, Morris D.: Performance Characteristics of Aircraft Cooling Ejectors Having Short Cylindrical Shrouds. NACA RM E51E01, 1951.

12. Vargo, Donald J.: Effects of Secondary-Air Flow on Annular Base Force of a Supersonic Airplane. NACA RM E54G28, 1954.

13. Hearth, Donald P., and Perchonok, Eugene: Analysis of Heat Addition in a Convergent-Divergent Nozzle. NACA TN 2938, 1953.

14. Krull, H. George, and Steffen, Fred W.: Performance Characteristics of One Convergent and Three Convergent-Divergent Nozzles. NACA RM E52H12, 1952.

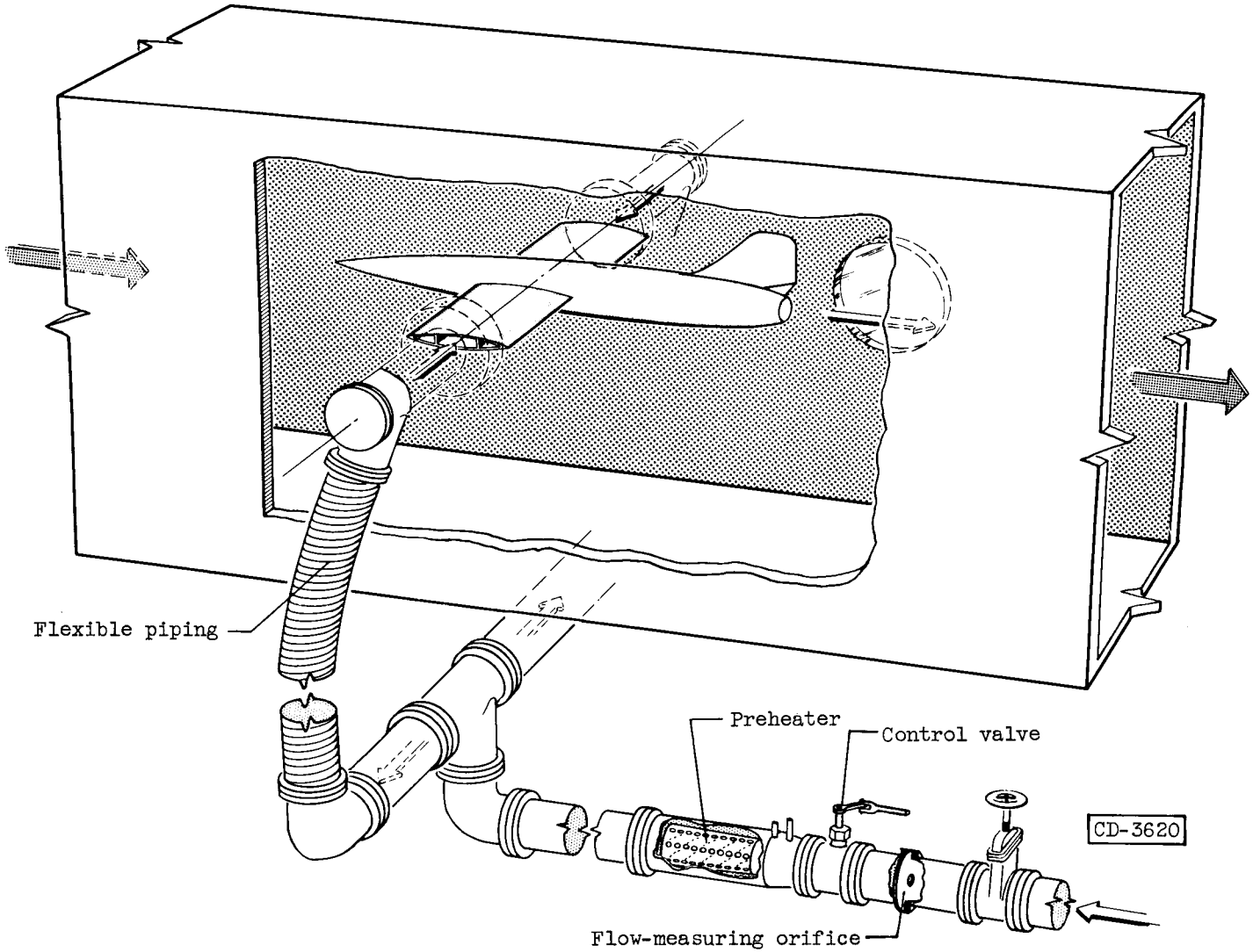

Figure 1. - Jet exit model installed in 8- by 6-foot supersonic wind tunnel.

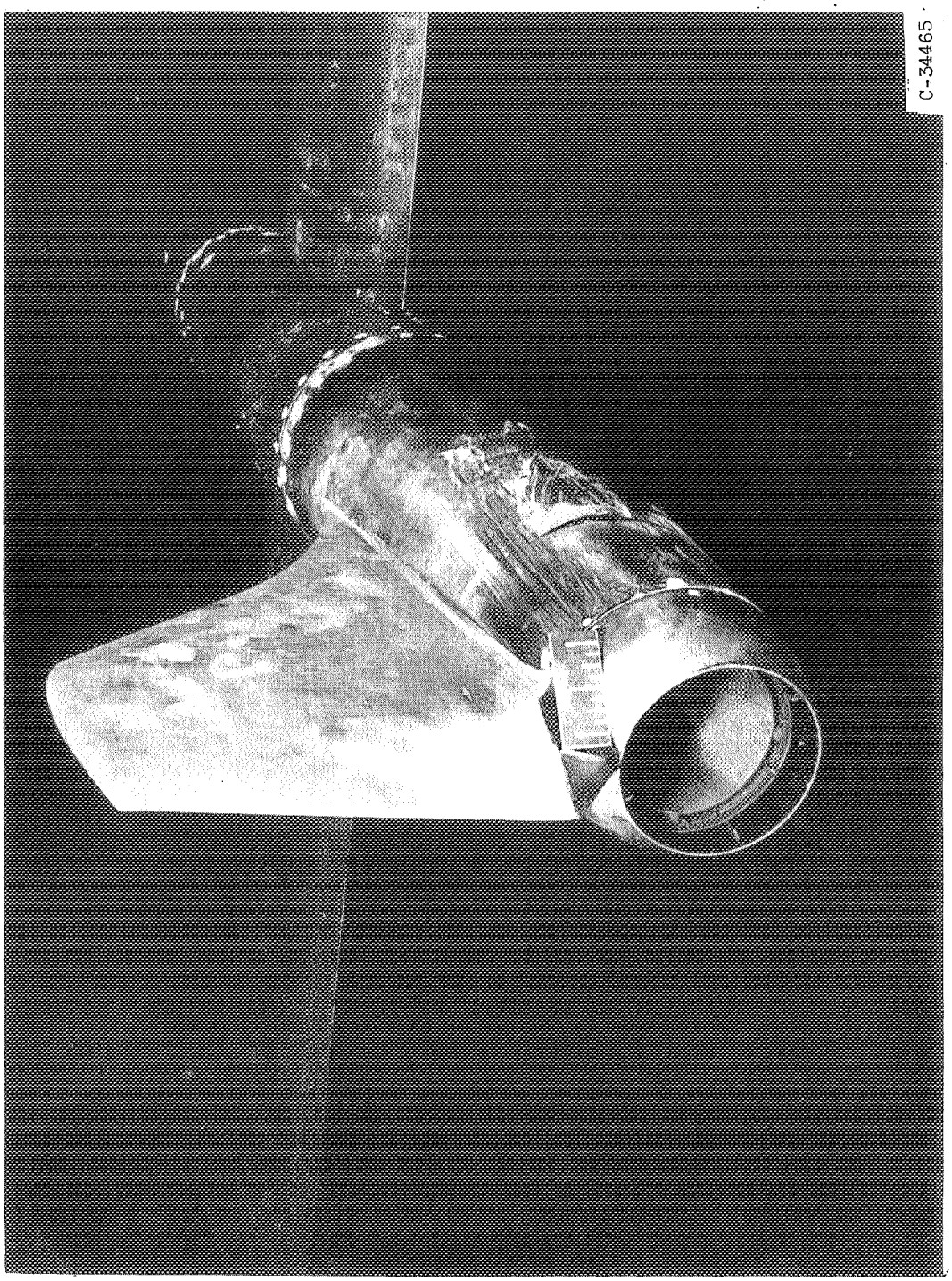

Figure 2. - Exit model in 8- by 6-foot tunnel.

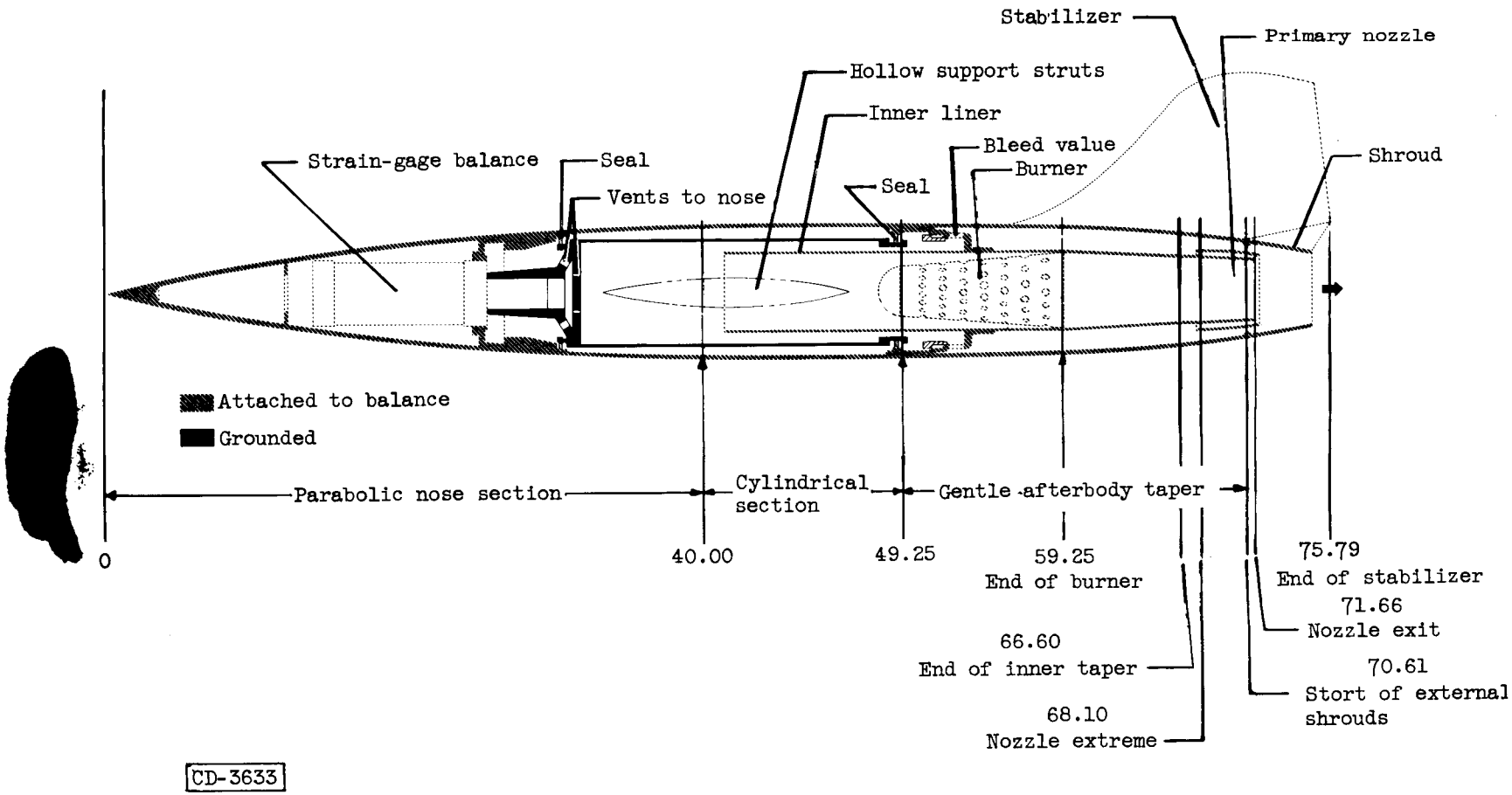

Figure 3. - Jet exit model. (All dimensions are in inches.)

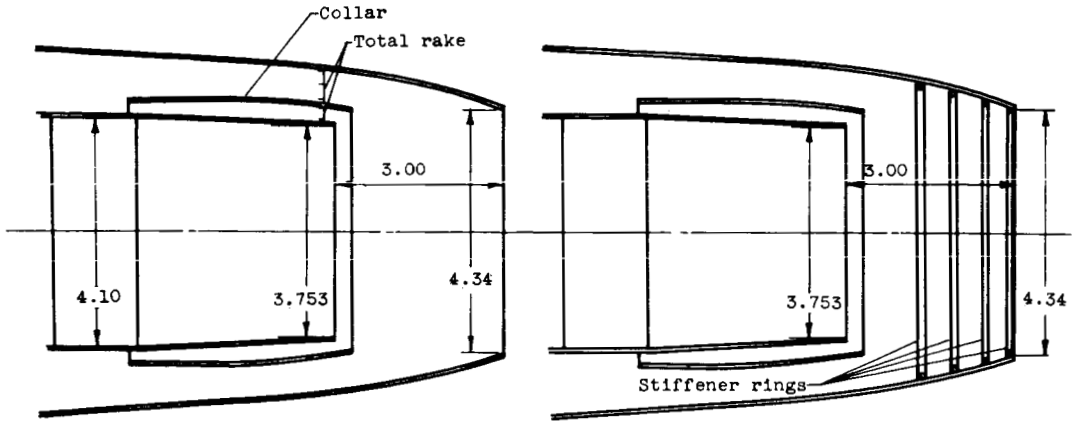

Ejector 1.16-0.80 $\left(\frac{ds}{dp} = 1.156, \frac{S}{dp} = 0.799\right)$ Ejector 1.16-0.80-S $\left(\frac{ds}{dp} = 1.156, \frac{S}{dp} = 0.799\right)$

Fuselage station	Inside diameter
70.61	5.74
71.66	5.55
72.72	5.26
73.77	4.86
74.75	4.34

(a) Ejectors 1.16-0.80 and 1.16-0.80-S.

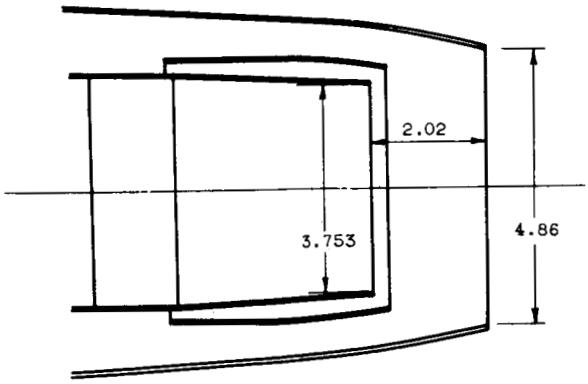

Fuselage station	Inside diameter
70.61	5.74
71.66	5.55
72.72	5.26
73.77	4.86

(b) Ejector 1.29-0.54 $\left(\frac{ds}{dp} = 1.295, \frac{S}{dp} = 0.538\right)$.

Figure 4. - Sketches and pertinent dimensions of configurations investigated. (All dimensions are in inches.)

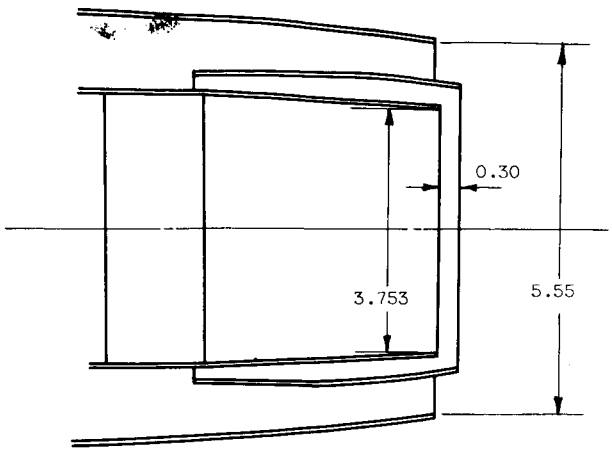

Fuselage station	Inside diameter
70.61	5.74
71.66	5.55

(c) Ejector 1.48-0 $\left(\frac{ds}{dp} = 1.479, \frac{S}{dp} = 0\right)$.

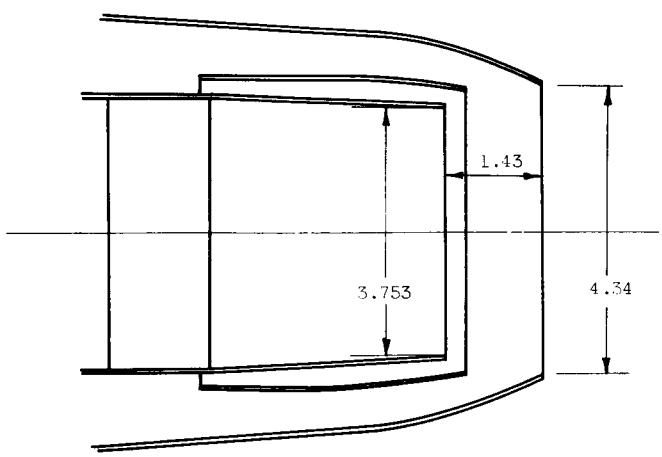

Fuselage station	Inside diameter
70.61	5.74
71.15	5.63
71.66	5.43
72.20	5.15
72.72	4.75
73.18	4.34

(d) Ejector 1.16-0.38 $\left(\frac{ds}{dp} = 1.156, \frac{S}{dp} = 0.381\right)$.

Figure 4. - Concluded. Sketches and pertinent dimensions of configurations investigated. (All dimensions are in inches.)

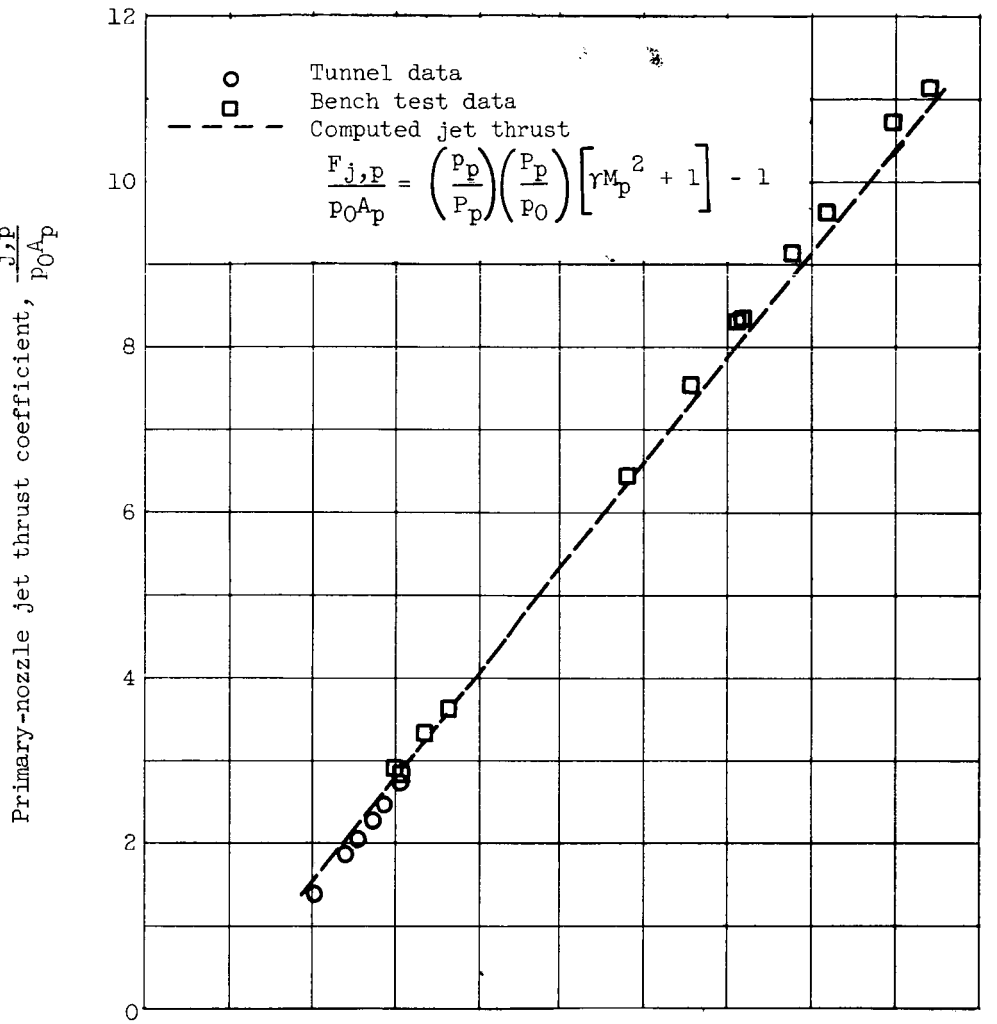

(a) Primary-nozzle jet thrust characteristics.

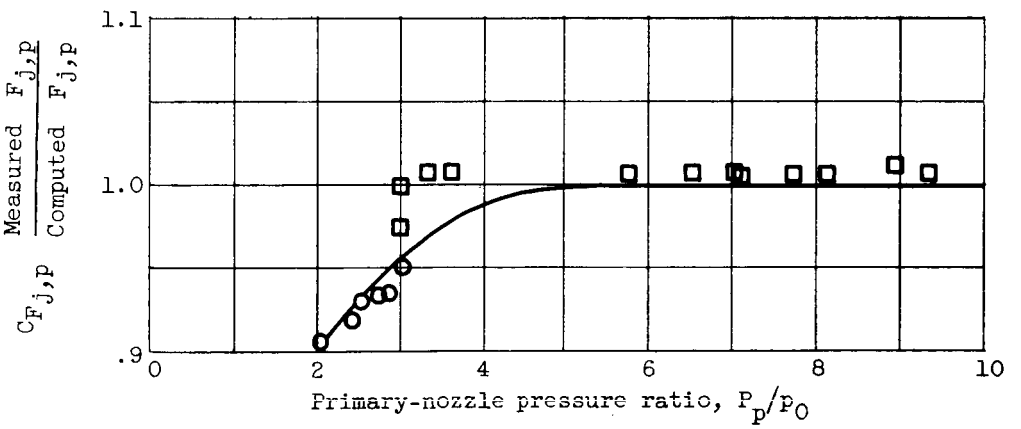

(b) Comparison of measured to computed primary jet thrust.

Figure 5. - Cali[redacted]ted primary-nozzle jet thrust.

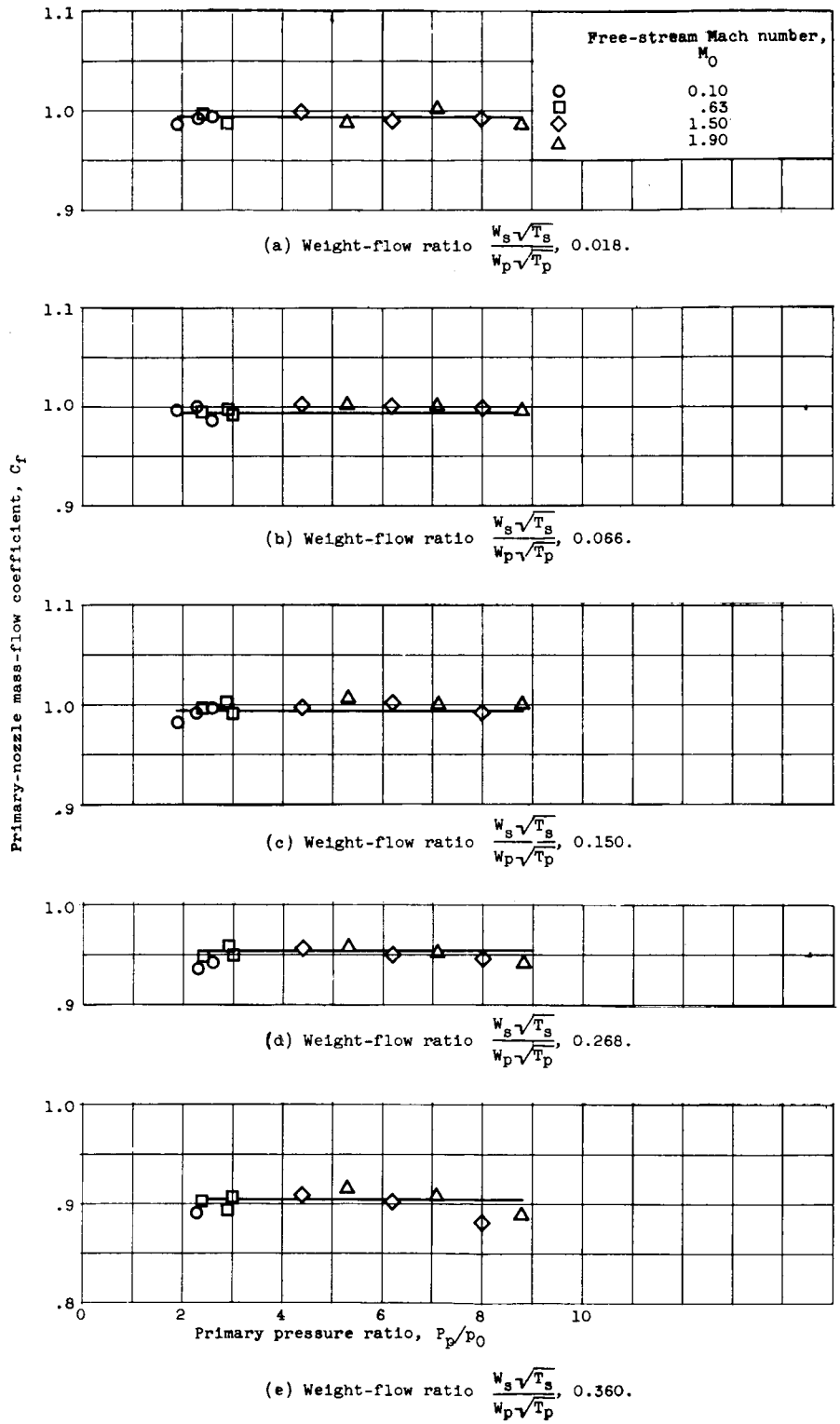

(a) Weight-flow ratio $\frac{W_s\sqrt{T_s}}{W_p\sqrt{T_p}}$, 0.018.

(b) Weight-flow ratio $\frac{W_s\sqrt{T_s}}{W_p\sqrt{T_p}}$, 0.066.

(c) Weight-flow ratio $\frac{W_s\sqrt{T_s}}{W_p\sqrt{T_p}}$, 0.150.

(d) Weight-flow ratio $\frac{W_s\sqrt{T_s}}{W_p\sqrt{T_p}}$, 0.268.

(e) Weight-flow ratio $\frac{W_s\sqrt{T_s}}{W_p\sqrt{T_p}}$, 0.360.

Figure 6. - Primary-nozzle mass-flow-coefficient characteristics. Ejector 1.16-0.80-S.

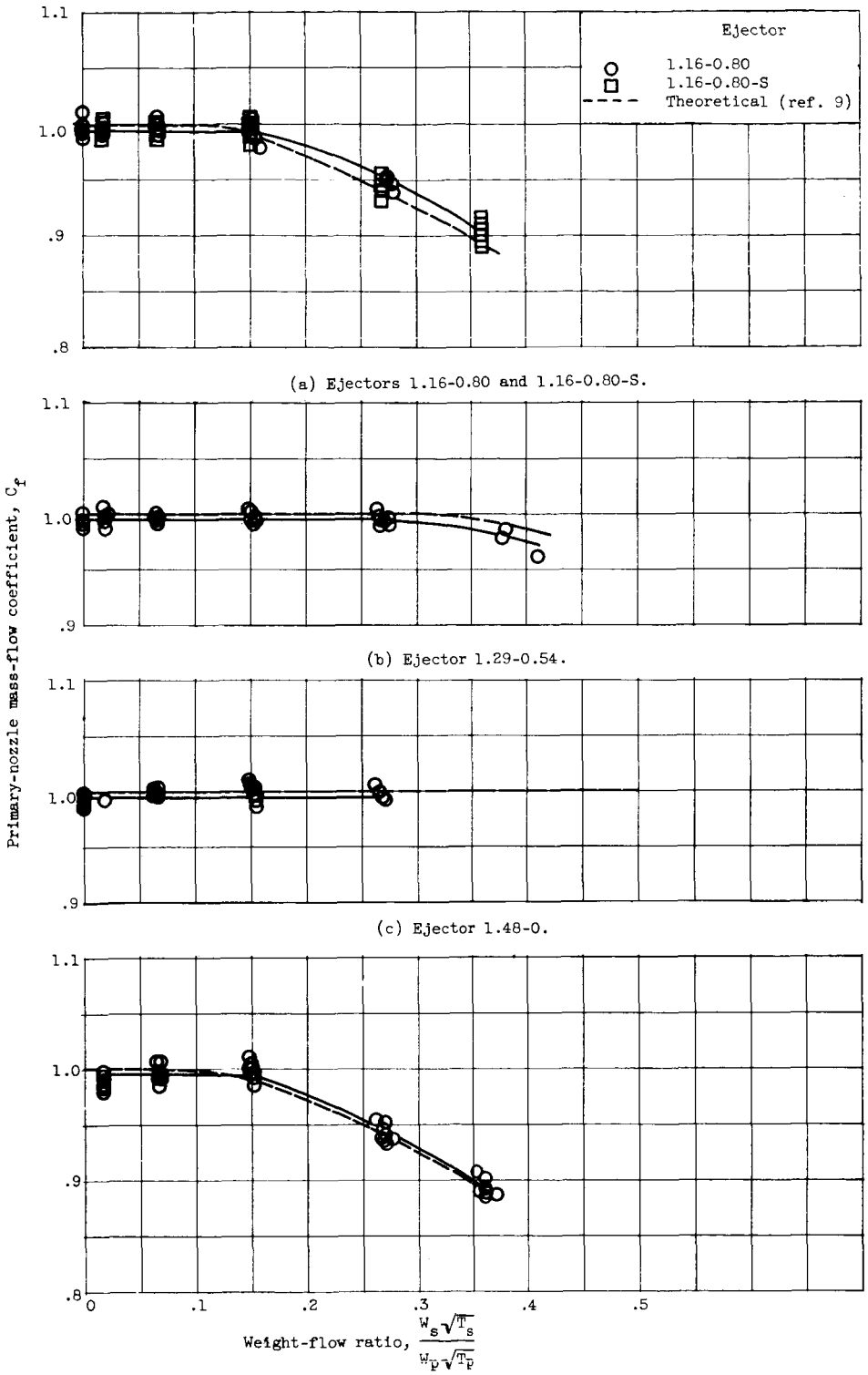

(a) Ejectors 1.16-0.80 and 1.16-0.80-S.

(b) Ejector 1.29-0.54.

(c) Ejector 1.48-0.

(d) Ejector 1.16-0.38.

Figure 7. - Effect of secondary weight flow on primary-nozzle mass-flow coefficient.

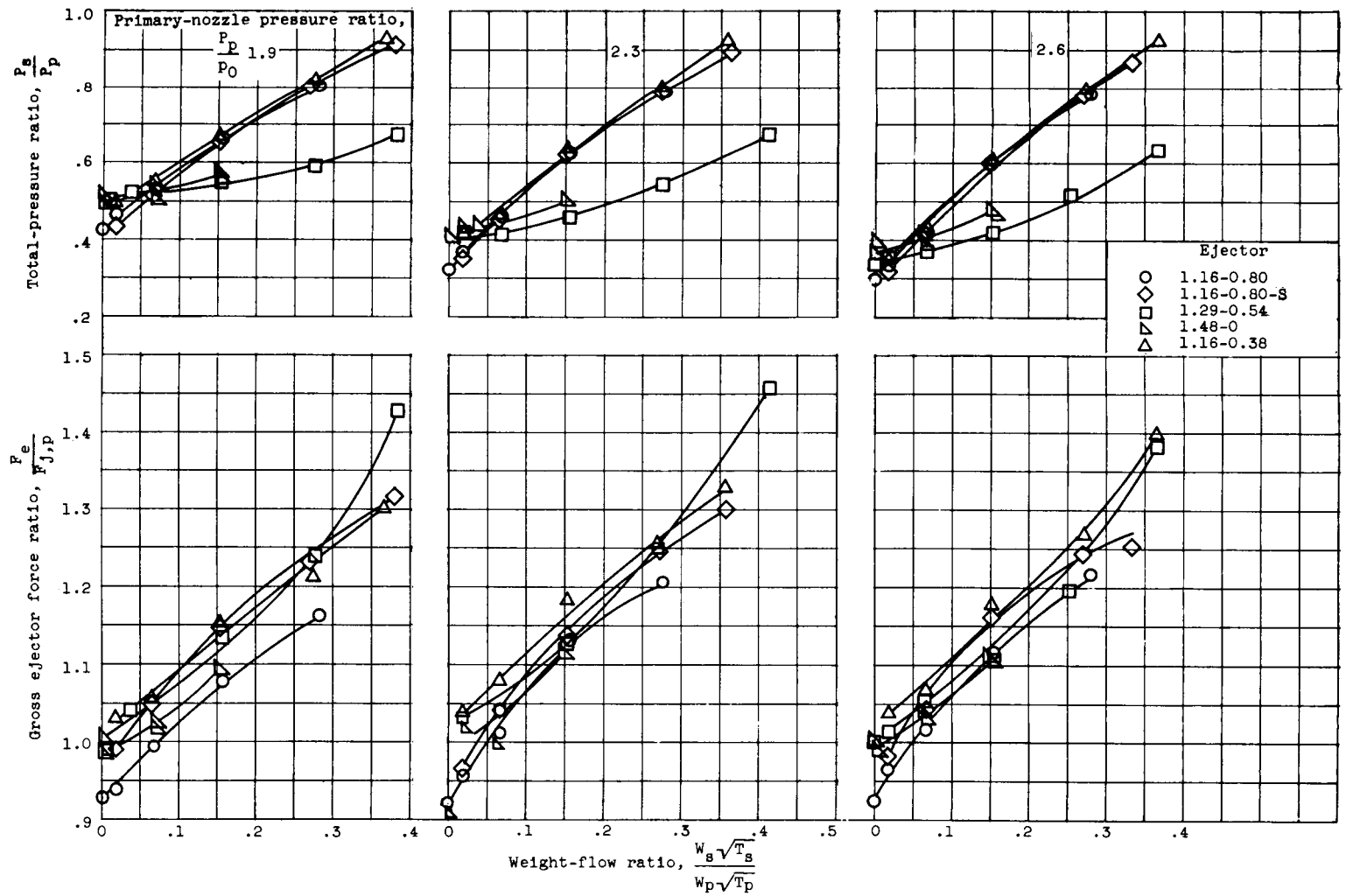

(a) Free-stream Mach number, 0.10.

Figure 8. - Gross ejector force and pumping characteristics.

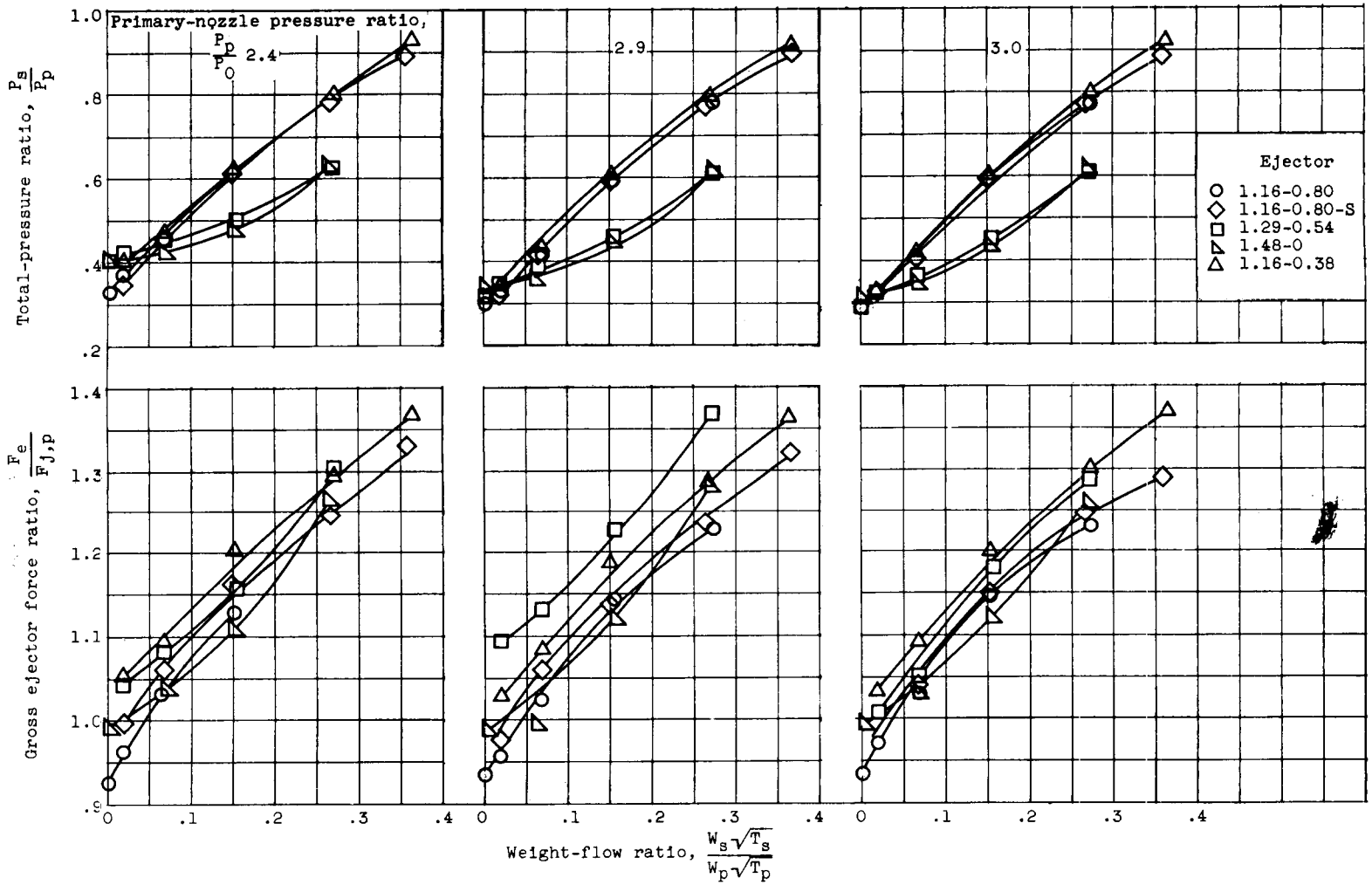

(b) Free-stream Mach number, 0.63.

Figure 8. - Continued. Gross ejector force and pumping characteristics.

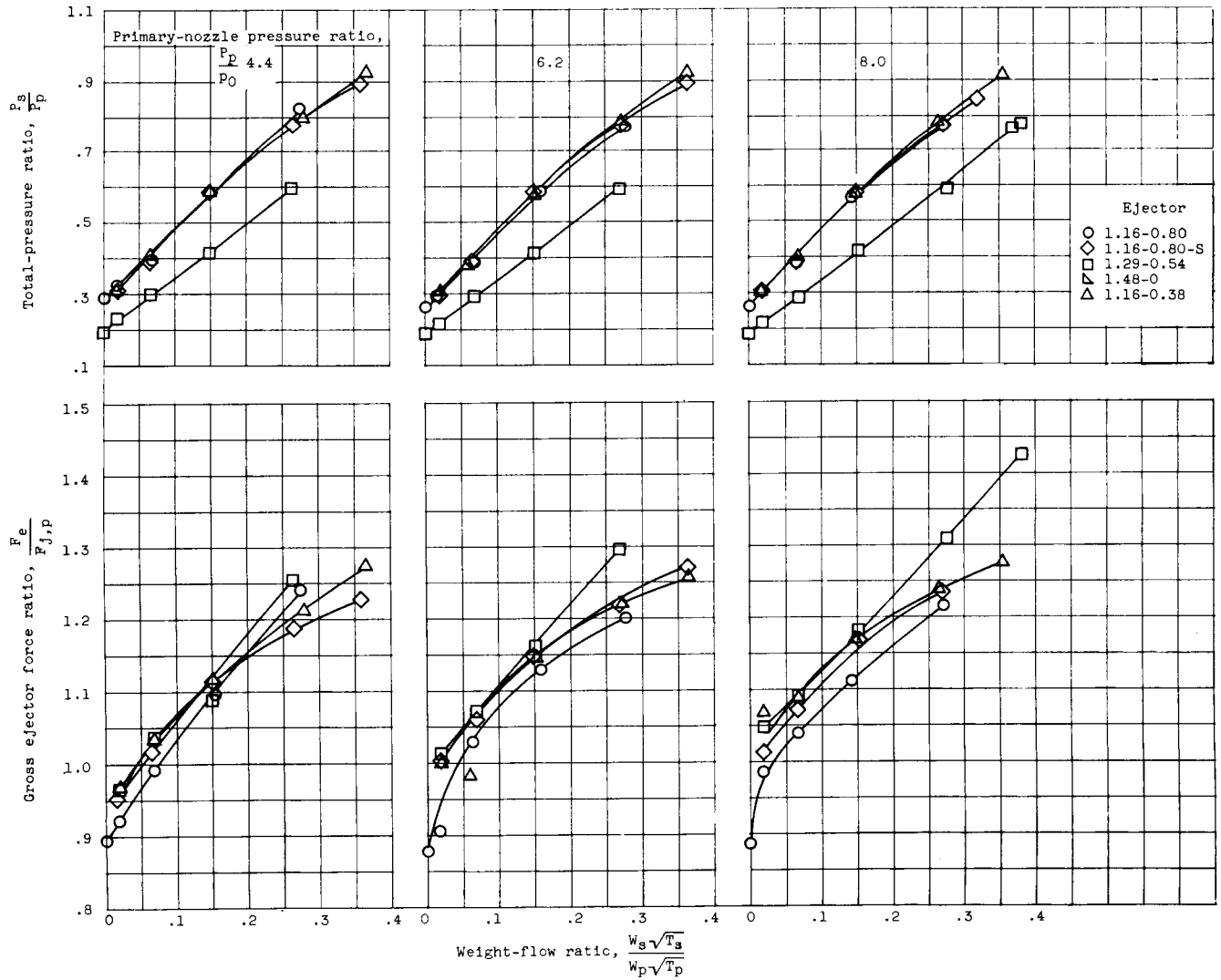

(c) Free-stream Mach number, 1.50.

Figure 8. - Continued. Gross ejector force and pumping characteristics.

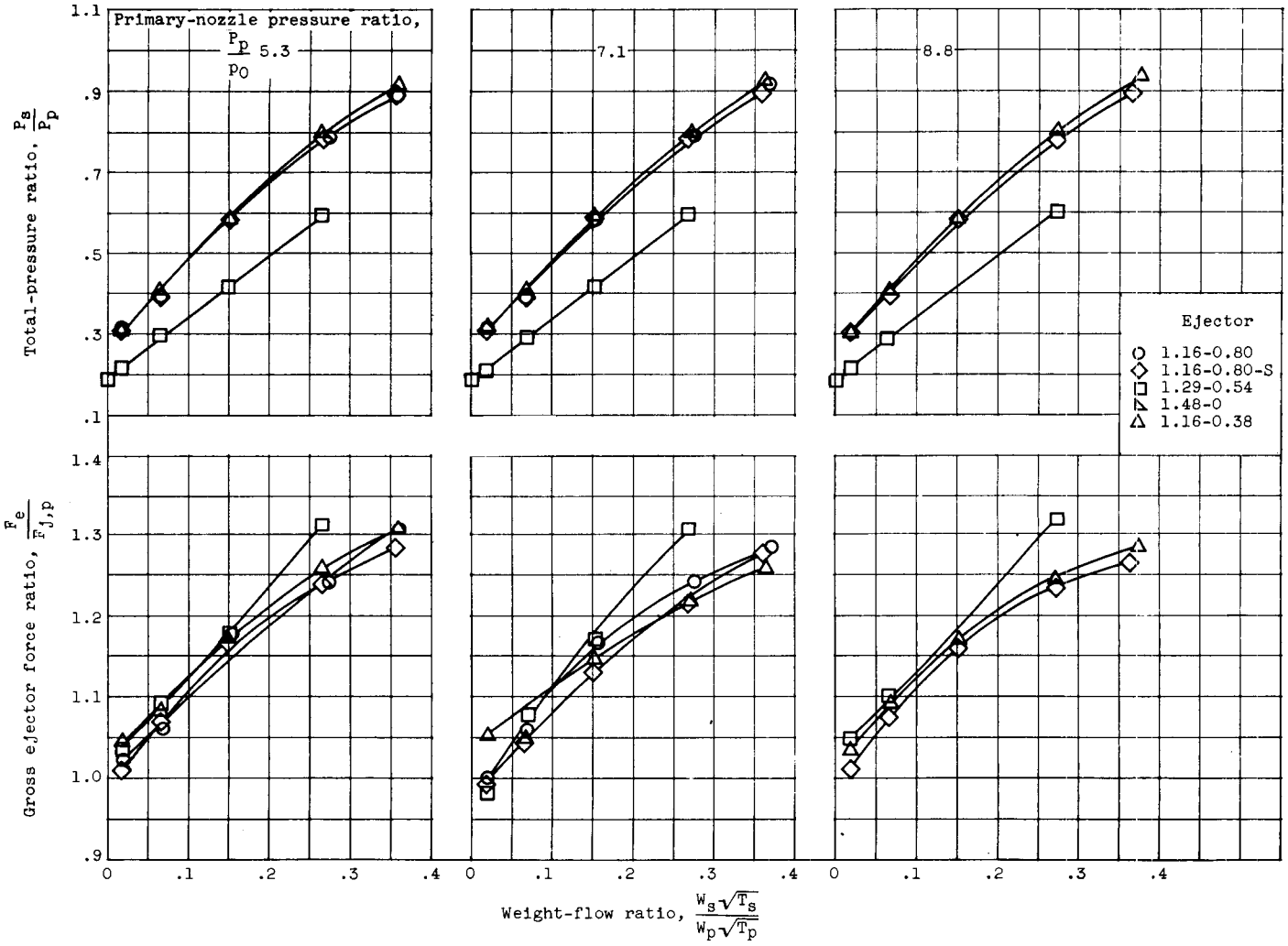

(d) Free-stream Mach number, 1.90.

Figure 8. - Concluded. Gross ejector force and pumping characteristics.

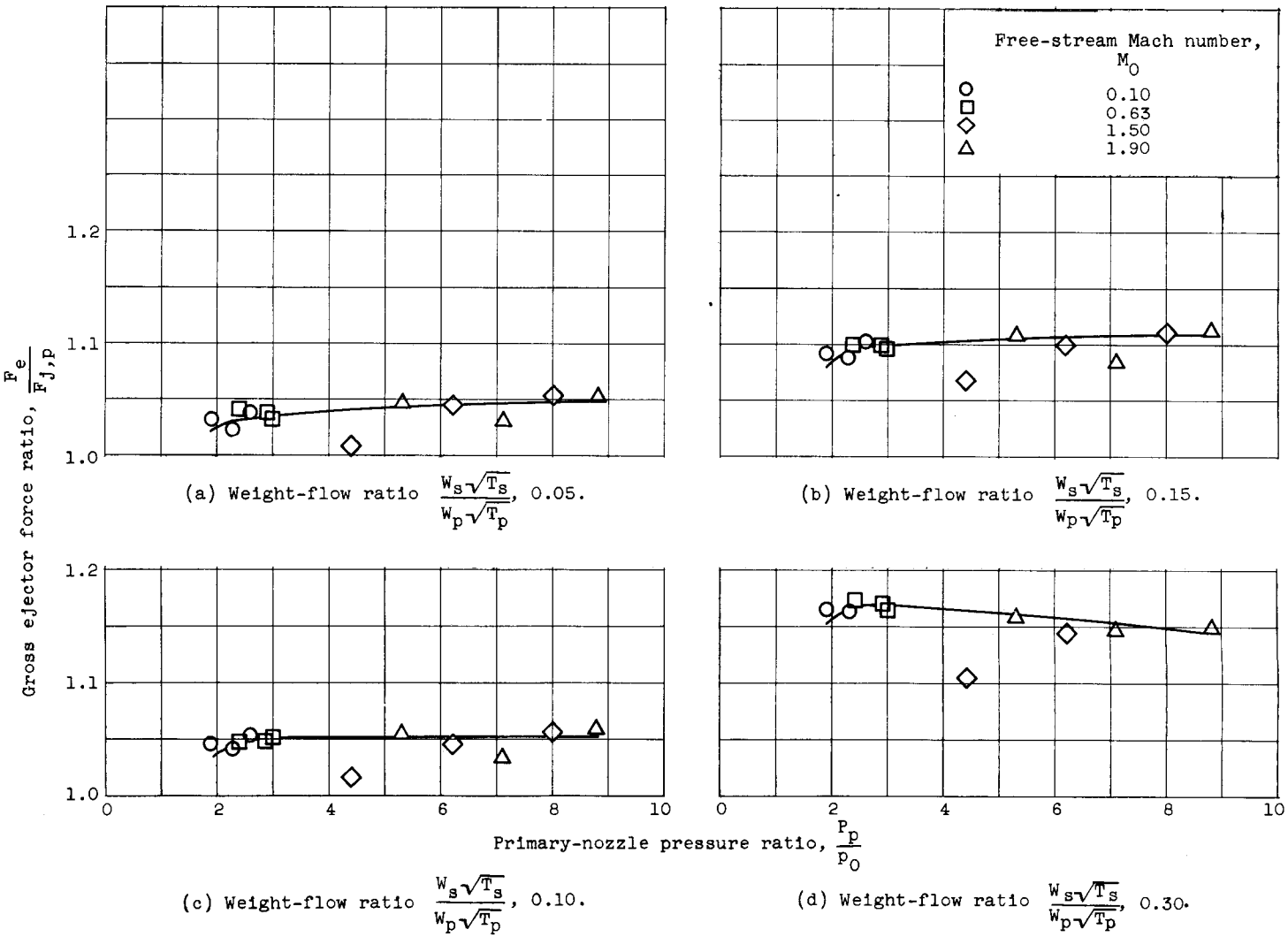

Figure 9. - Effect of free-stream Mach number on gross ejector force ratio for ejector 1.16-0.80-S.

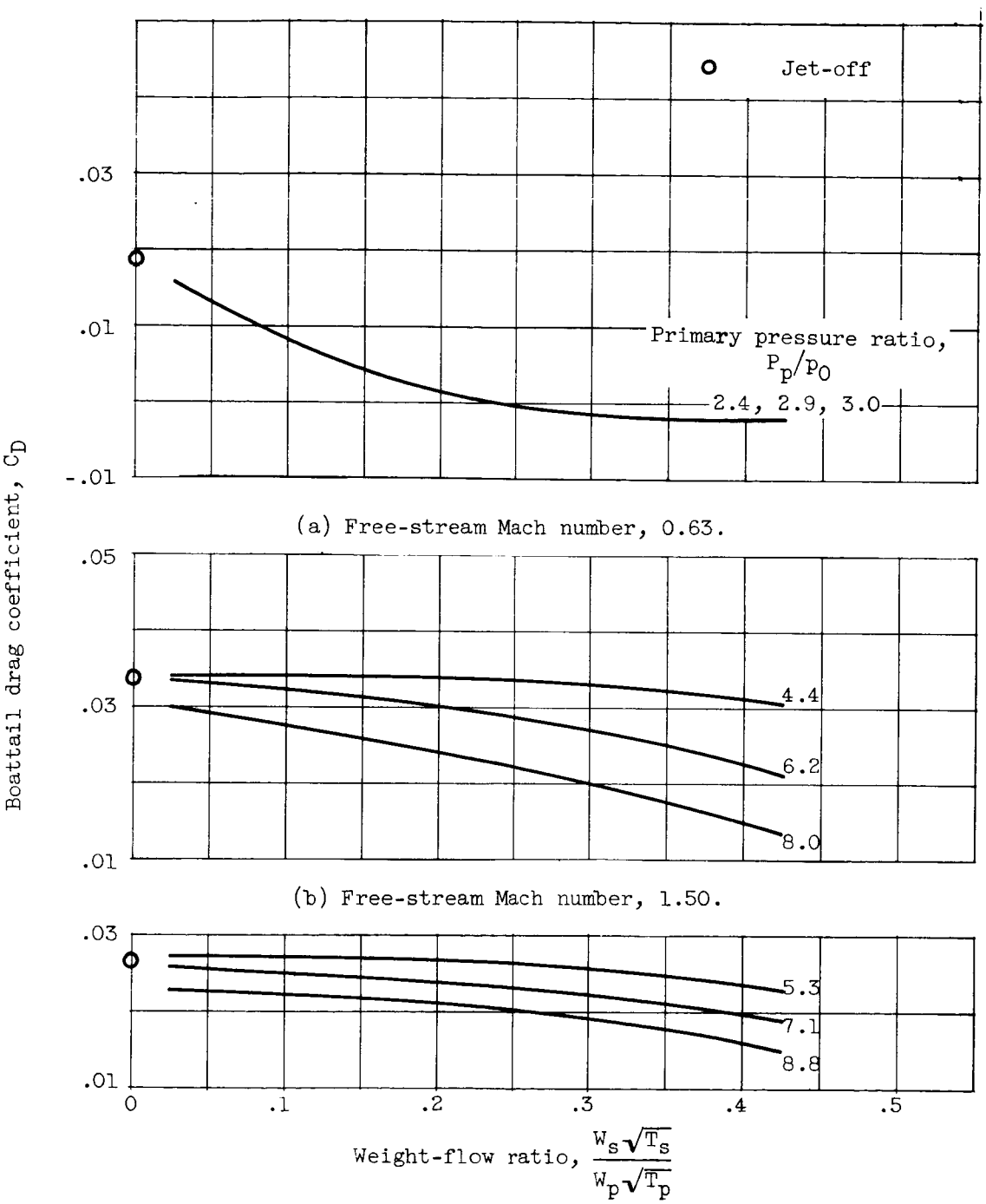

(a) Free-stream Mach number, 0.63.

(b) Free-stream Mach number, 1.50.

(c) Free-stream Mach number, 1.90.

Figure 10. - Estimated boattail drag characteristics.

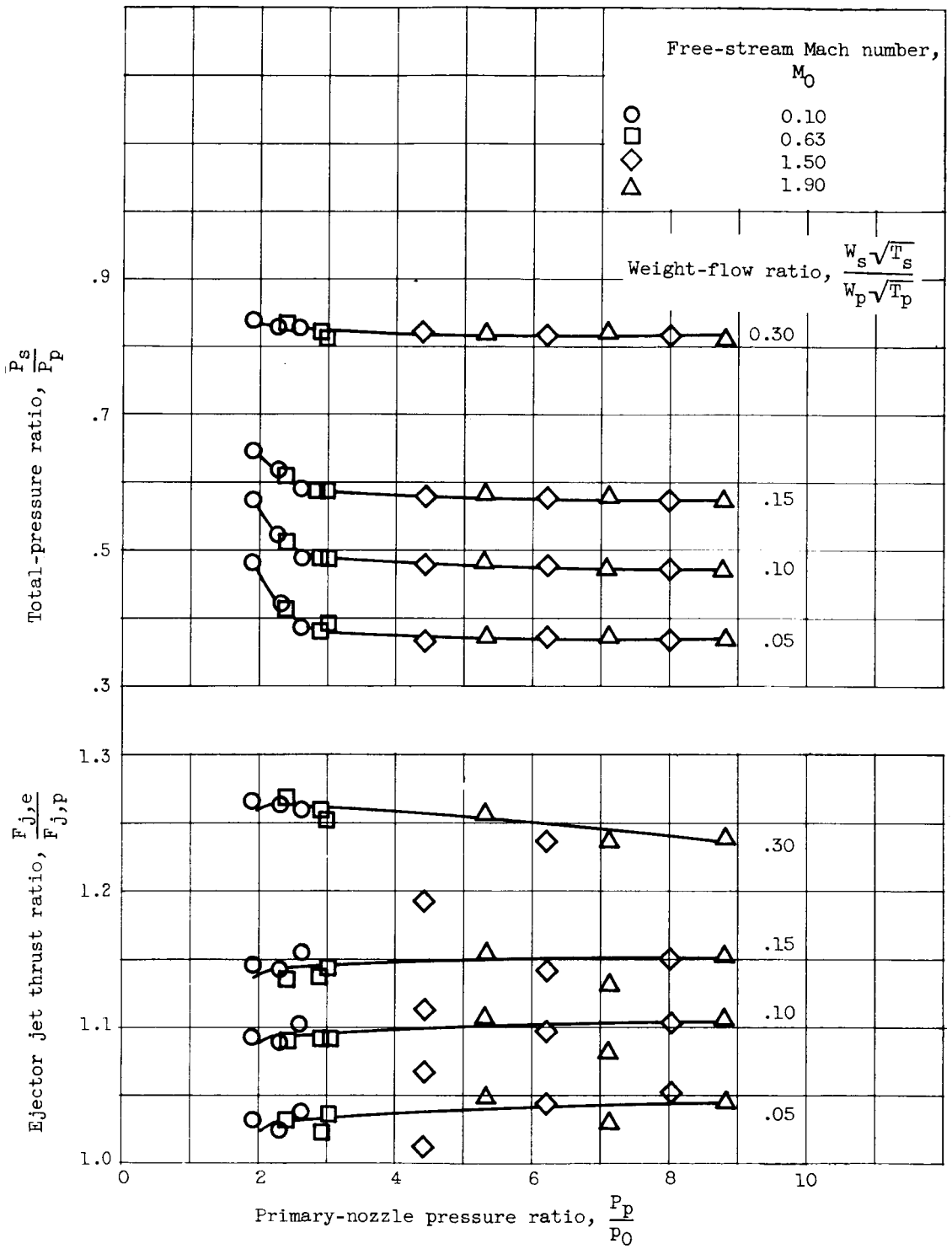

Figure 11. - Effect of free-stream Mach number on pumping and ejector jet thrust characteristics for ejector 1.16-0.80-S.

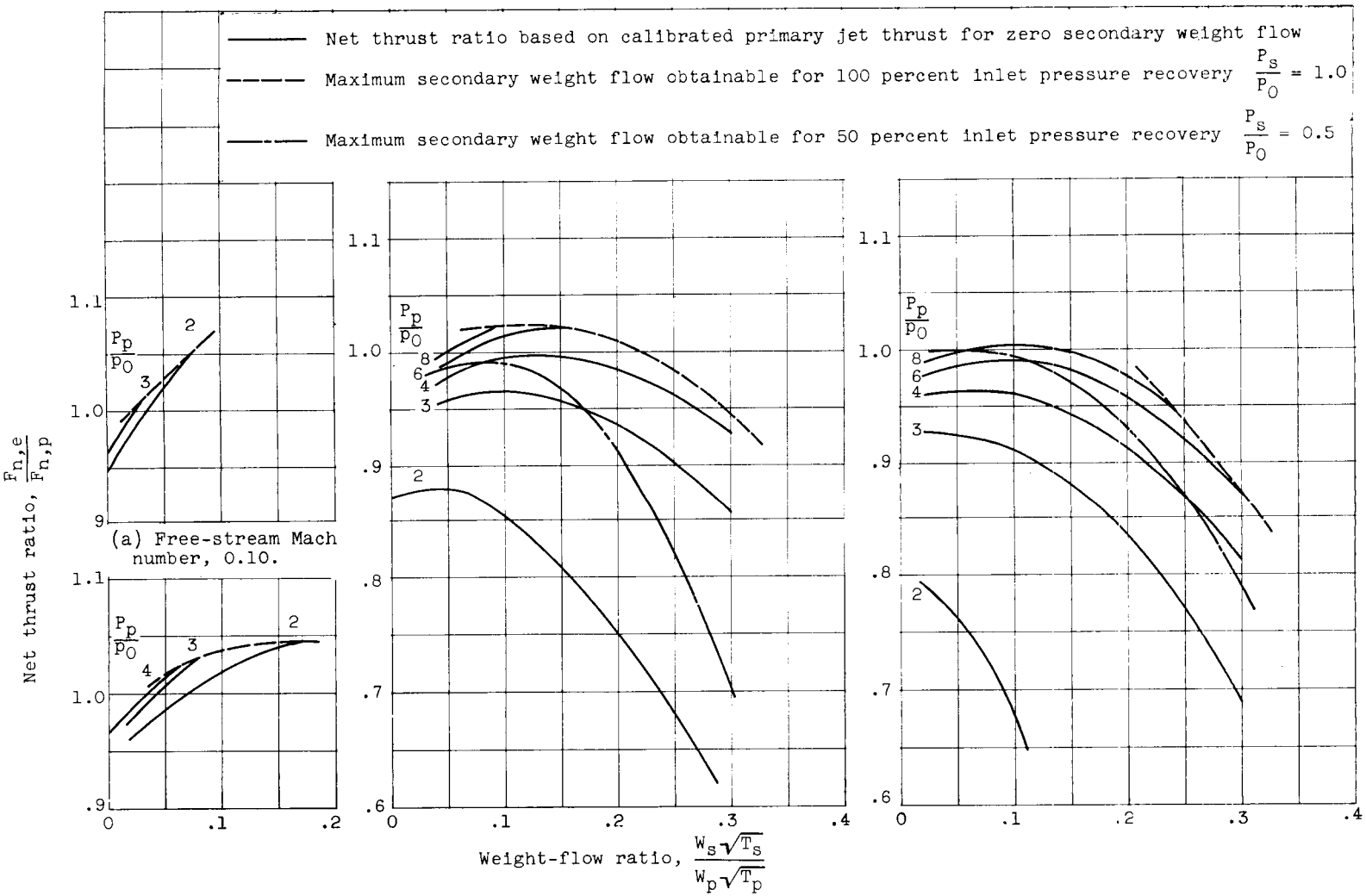

(a) Free-stream Mach number, 0.10.

(b) Free-stream Mach number, 0.63.

(c) Free-stream Mach number, 1.50.

(d) Free-stream Mach number, 1.90.

Figure 12. - Net thrust characteristics for ejector 1.16-.80-S.

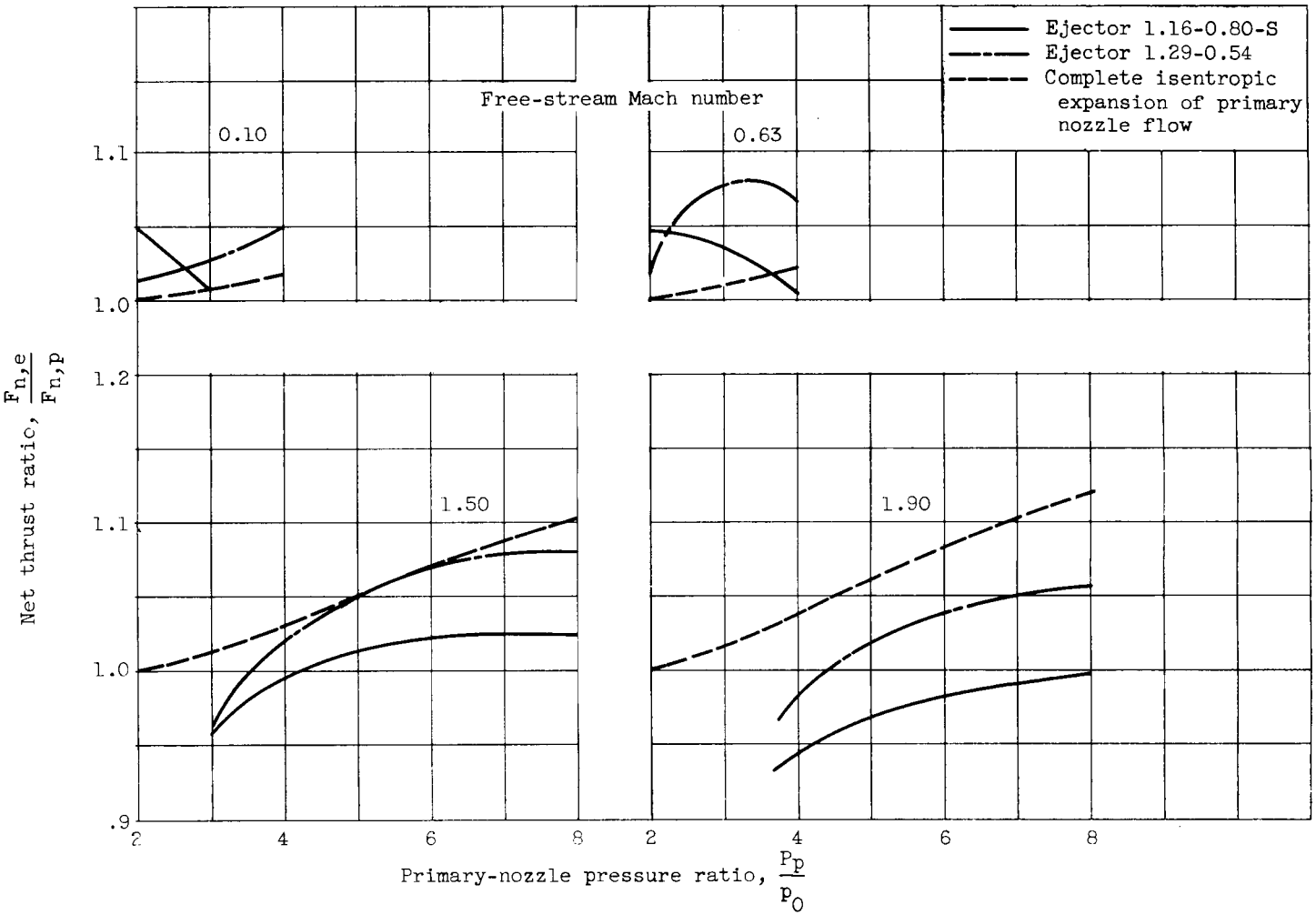

Figure 13. - Comparison of methods for net thrust augmentation of primary nozzle. Weight-flow ratio $\frac{W_s\sqrt{T_s}}{W_p\sqrt{T_p}}$, 0.15 or at $\frac{P_s}{P_0}$ = 1.00 if limited.

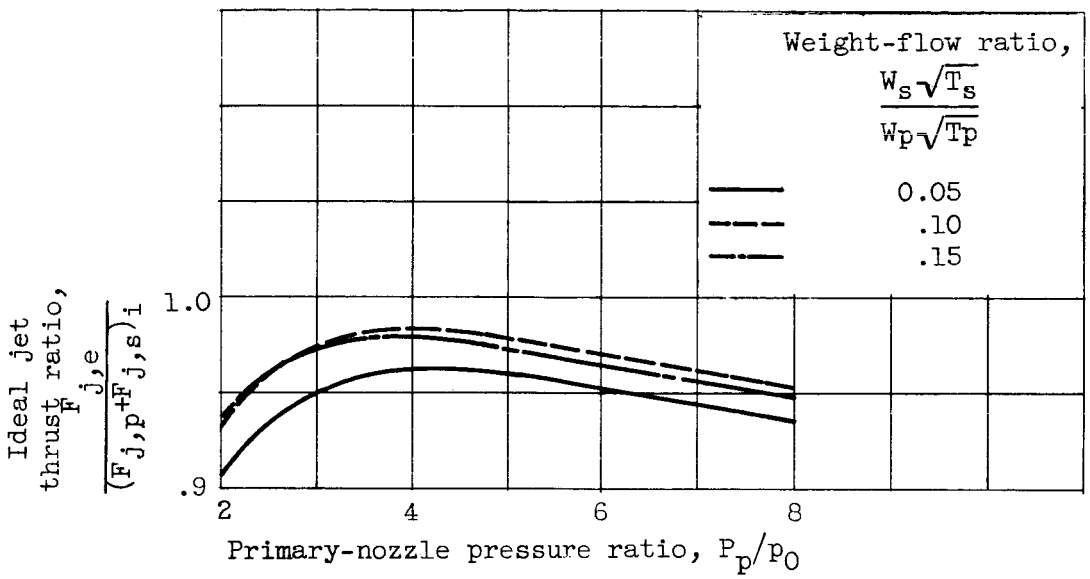

Figure 14. - Ideal jet thrust characteristics for ejector 1.16-0.80-S.